Self-collimating polarization beam splitter based on photonic crystal Mach–Zehnder interferometer

Yi Xu, Shun Wang, Sheng Lan, Xu-Sheng Lin, Qi Guo, and Li-Jun Wu*

Laboratory of Photonic Information Technology, School for Information and Optoelectronic Science and Engineering, South China Normal University, Guangzhou 510006, People's Republic of China
**Corresponding author: ljwu@scnu.edu.cn*

Received December 17, 2009; revised May 10, 2010; accepted May 10, 2010;
posted May 11, 2010 (Doc. ID 121696); published June 11, 2010

Due to different boundary continuity conditions, electromagnetic waves with transverse-magnetic and transverse-electric polarizations respond differently when they encounter dielectric interfaces. Based on this mechanism, we propose a self-collimating polarization beam splitter (PBS) constructed on a polarization-insensitive self-collimation photonic crystal. The splitting is realized on a Mach–Zehnder interferometer (MZI), through which the two polarizations can be separated by 90° with low cross talk. Both polarizations are self-collimated to eliminate the diffraction loss during the propagation. Furthermore, the out-of-plane scattering loss is suppressed since the PBS is operated in the first band. The wavelength bandwidth of the MZI-based PBS reaches about 100 nm at 1550 nm. Finally, the influences of interfaces on the performance of the PBS are discussed. © 2010 Optical Society of America

OCIS codes: 230.5440, 230.1360, 350.4238.

1. INTRODUCTION

Polarization beam splitters (PBSs) with low cross talk are essential components in photonic integrated circuits (PICs). Conventional PBSs such as those based on ridge waveguides typically require an interaction length of several millimeters and this requirement makes them less attractive for integration [1]. Photonic crystals (PhCs), because of their interesting dispersive properties, provide various opportunities to manipulate light waves in PICs. Polarization beam splitting is one of their potential applications in PICs. Several groups have demonstrated this function in PhCs. For example, Wu *et al.* separated two polarizations by utilizing the dispersion diversities of PhCs [2]. Ao *et al.* [3,4] and Schonbrun *et al.* [5] demonstrated PBS based on the polarization-dependent refraction and directional bandgap effect in PhCs, respectively. However, as the diffraction of electromagnetic (EM) waves leads to significant spreading as they propagate, the PBS realized by these methods suffers from diffraction loss. Self-collimating phenomenon in PhCs means that the energy propagation directions for all the excited modes are identical and the diffraction can be almost eliminated [6–9]. Based on this phenomenon, Zabelin *et al.* demonstrated a self-collimating PBS to cancel the diffraction effect. However, their device operates in the second band and suffers from intrinsic out-of-plane scattering loss [10].

As is known, the properties of PhCs are critically dependent on the shape of their unit cells. By tailoring the shape from a normally used circle to a pill, we have realized the polarization-independent self-collimation (SC) in a PhC with the symmetry of a square lattice [11]. By utilizing this special pill-void PhC structure, we propose and demonstrate a PBS constructed on a Mach–Zehnder interferometer (MZI). The transverse-magnetic [TM, the magnetic-field (*H*-field) parallel to the plane] and transverse-electric [TE, the electric-field (*E*-field) parallel to the plane] polarizations can be separated by 90° in a structure as short as 13 μm (1550 nm regime). Both polarizations are self-collimated to eliminate the diffraction loss. Furthermore, the out-of-plane scattering loss is suppressed since the PBS is operated in the first band.

2. THE MECHANISM OF MACH–ZEHNDER INTERFEROMETER POLARIZATION BEAM SPLITTER

In isotropic and uniform media, the behavior of the TE- and TM-polarized waves is the same. When they encounter a change in the permittivity (we assume the relative permeability $\mu=1$ as most of the materials in PICs are non-magnetic), the *H*-field and *E*-field undergo different variations. Normally, the *H*-field can be considered to be both normal- and tangent-continuous through interface in a non-magnetic material for both polarizations. For the TM polarization, the *E*-field is parallel to the interface and is tangent-continuous. It does not have any normal component. In the TE case, however, the boundary continuity situation is different. As the displacement field *D* is normal-continuous at the interface, the *E*-field is forced to cross different dielectrics and is thus non-continuous at the interface. As a result, the responses from TE and TM polarizations are different.

If we introduce a very narrow gap such as a subwavelength air slit into a medium with a high dielectric constant (for example, $\varepsilon=11.56$), as shown in the inset of Fig. 1, the propagation behavior of the TE- and TM-polarized waves will be different when the width of the slit is less than 300 nm. We employ a numerically stable enhanced transmittance approach to calculate the transmission/

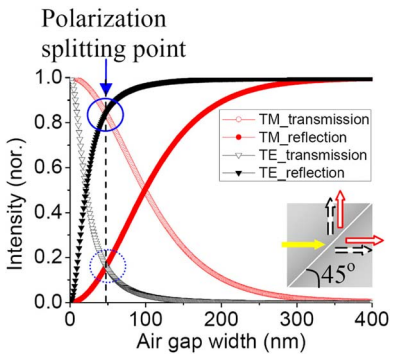

Fig. 1. (Color online) The transmission and reflection of both polarizations when light travels through a dielectric-air-dielectric sandwich structure at an angle of 45°. The red solid (black dashed) color represents the TM (TE) polarization in the whole article unless specified. Open shapes denote the transmission and bulk ones indicate the reflection. The inset is the sketch of the dielectric-air-dielectric (in gray-white-gray) sandwich structure.

reflection of the TE/TM polarizations and analyze their difference since it is based on the continuity of the tangential component of the EM field at interfaces [12]. As outlined in the inset of Fig. 1, TE- and TM-polarized plane waves at a wavelength of 1550 nm impinge on the air slit from the left-hand side at an angle of 45°, which is greater than the critical angle. If the air gap is much wider than the skin depth of the evanescent field, both the TE and TM polarizations will be totally internal reflected and decay exponentially along the normal of the interface in air. However, if the width of the air gap is reduced to subwavelength, optical tunneling will occur.

The calculation results are displayed in Fig. 1. As can be seen, the TE (TM) polarization is split equally into reflection and transmission at the air gap with a width (d) of 20 (100) nm. With an increase in d, the TE polarization is totally internal reflected before TM polarization. Therefore, the width of the air gap may be designed in such a way that the TM polarization tunnels through while the TE is reflected. From Fig. 1, the separation between TE and TM polarizations is obvious (at the point blue circled). With a single air slit, it is not surprising to find that the cross talk is high (about 20%) for both polarizations.

As a MZI consists of two beam splitters and two reflecting mirrors [13], we utilize this configuration to realize the function of splitting. In order to suppress the propagating loss induced by the diffraction, we construct the MZI on a pill-void PhC with a square symmetry, which has been shown to be able to collimate both polarizations [11]. Figure 2(a) presents the equi-frequency contours (EFCs) (calculated by the plane-wave expansion method) of the PhC structure, in which the pill-shape voids are drilled in GaAs ($\varepsilon=11.56$). The structural parameters of the PhC are described in the caption of Fig. 2. A freely available software package was employed to obtain the fully vectorial eigenmode solutions of the Maxwell's equations [14]. 4096 plane waves were used to obtain convergent results. By analyzing the EFCs, it can be found that both TE and TM polarizations with ±6° divergence can be collimated along the ΓM and ΓM_2 directions with a frequency bandwidth of ~6.5%. This angular range (±6°) is larger than the divergence of a common single mode fiber.

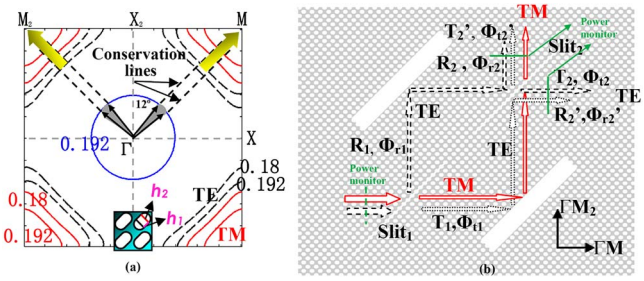

Fig. 2. (Color online) (a) The EFCs for the pill-void square lattice with $h_1=0.2a$, $h_2=0.6a$, where a is the lattice constant. As can be seen, the propagation directions of the energy, which are perpendicular to the EFCs, are along the ΓM and ΓM_2 directions in PhCs when the divergence of the incident beams is within 12° (i.e., ±6°) and the frequency is among 0.18–0.192 ($\times 2\pi c/a$) (shown in yellow bulk arrows). (b) The sketch of the MZI-based PBS. The TM-polarized beam mainly transmits through the two air slits along the red solid arrows. At slit 1, The TE-polarized beam is partially reflected (R_1, in black dashed arrow) and transmitted (T_1, in black dotted arrow). At slit 2, the reflected and transmitted part is partially reflected (R_2,R_2') and transmitted (T_2,T_2') again. ($\Phi_{r2}-\Phi_{t2}'$) represents the PD between the two beams reflected and transmitted by slit 2 at the upper port, while ($\Phi_{r2}'-\Phi_{t2}$) represents that between those reflected and transmitted at the right port. The green lines represent the positions of the power monitor.

Figure 2(b) shows the sketch of the MZI-based PBS constructed on such kind of PhCs. Two air slits, which can function as line defects to split beams in PhCs [15], are utilized to perform as splitters in the MZI. Its width is designed in such a way that the TM polarization can tunnel through while the TE polarization is partially reflected and transmitted. Then the TM polarization travels along the solid red arrows and propagates out mainly from the upper port at last. For the TE polarization, if the interference between the reflected and transmitted waves at the upper port is destructive while that at the right port is constructive, it will propagate out only from the right port.

The output of the TE polarization in a symmetric MZI can be expressed as in [13],

$$I_{\text{upper}} = A^2(1 - R_1 - R_2' + R_1R_2 + R_1R_2' + 2\sqrt{T_1T_2'R_1R_2}\cos((\phi_{r1} - \phi_{t1}) + (\phi_{r2} - \phi_{t2}'))), \quad (1)$$

$$I_{\text{right}} = A^2(R_1 + R_2' - R_1R_2 - R_1R_2' + 2\sqrt{T_1T_2R_1R_2'} \times\cos((\phi_{r1} - \phi_{t1}) - (\phi_{r2}' - \phi_{t2}))), \quad (2)$$

where I_{upper} (I_{right}) represents the light intensity at the upper (right) port and A stands for the amplitude of the magnetic field. R_1 and T_1 are the reflectance and transmittance at slit 1, while (R_2,R_2') and (T_2,T_2') are those at slit 2 as shown in Fig. 2(b). ($\Phi_{r1}-\Phi_{t1}$) represents the phase difference (PD) between the reflected and transmitted waves induced by slit 1. ($\Phi_{r2}-\Phi_{t2}'$) and ($\Phi_{r2}'-\Phi_{t2}$) denote the PD between two beams at the upper and right ports when two in-phase sources impinge slit 2 along the ΓM and ΓM_2 directions simultaneously. More descriptions for these parameters can be found in the caption of Fig. 2. As the PD and power-splitting ratio at the two slits can-

not be obtained analytically, these two equations are semi-analyzing solutions. The two-dimensional finite-difference time-domain (FDTD) method is employed to obtain them numerically. In the numerical experiments, we use a uniaxial anisotropic perfect match layer boundary condition [16] in all the calculations in this paper without restatement. All the PDs are measured at the same optical path. As the phase shift induced by the two reflecting mirrors is similar, whether the beam is incident on the ΓM or ΓM_2 direction (the results are not shown), we only consider the influence of the two slits in the calculations. The results are shown in Fig. 3, where the two insets in Figs. 3(c) and 3(d) display the configuration of the two slits. To resolve the narrow air slits, the grid size is set to $a/50$ in all the FDTD calculations unless specified, where a is the lattice constant of the PhC. We only present the modeling results at a normalized frequency of 0.188 $\times 2\pi c/a$ as an example. The results are similar at other frequencies as the width of the slits is much smaller than the operating wavelength and they are insensitive to the change in the wavelength. As can be seen in Figs. 3(a) and 3(b), $(\Phi_{r1}-\Phi_{t1})$, $(\Phi_{r2}-\Phi_{t2}')$, and $(\Phi_{r2}'-\Phi_{t2})$ remain at $\sim 90°$ when the width of the air slit varies from $0.1a$ to $0.4a$. From Figs. 3(c) and 3(d), it can be found that $T_1R_2' \approx T_2'R_1$. As a result, the relationship $I_{\text{upper}}+I_{\text{right}} \approx 1$ can be deduced from Eqs. (1) and (2), meaning that the energy is basically conserved.

From the modeling results exhibited in Figs. 3(c) and 3(d), we also found that when the widths of slits 1 and 2 are $0.15a$ and $0.135a$, $1-R_1-R_2'+R_1R_2+R_1R_2' -2\sqrt{T_1T_2'R_1R_2}=0$. (Note that R_2/T_2 is the same as R_1/T_1 since their incident directions with respect to the slits are the same.) Combining this result with Eqs. (1) and (2), we can deduce that $I_{\text{upper}}=0$ and $I_{\text{right}}=1$, meaning that the reflected and transmitted beams (TE-polarized) at the upper port interfere destructively and only travel out from the right port. For the TM polarization, it is almost not perturbed by these two narrow slits and passes through at high transmission ($\sim 95\%$ at both slits 1 and 2). As a result, TE and TM polarizations are separated with low cross talk at slit 2. The different response of TE polarization between the two slits in Figs. 3(c) and 3(d) is due to the 180° rotation symmetry of the pill-void PhCs.

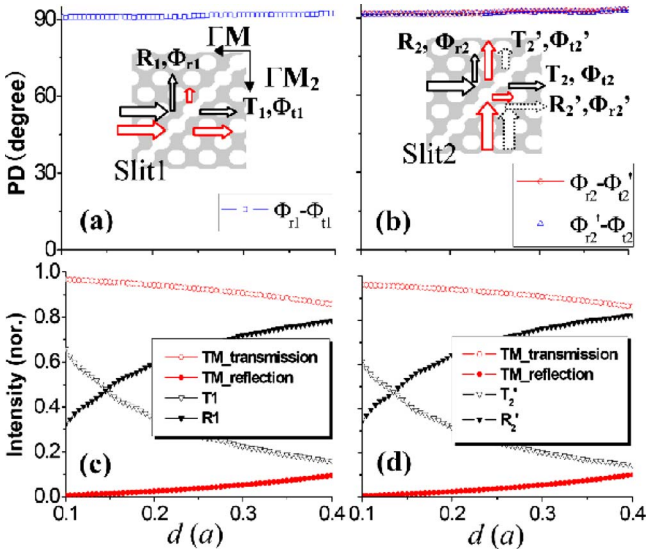

Fig. 3. (Color online) The PD induced by (a) slit 1 and (b) slit 2. The two insets show the configuration of the two air slits. The transmission and reflection of the incident beam along the ΓM direction are shown in (c) and those along the ΓM_2 direction are shown in (d). Note that R_2 and T_2 are the same as R_1 and T_1 as they are all normalized to their own incident directions (along the ΓM direction) of the slit.

3. FDTD NUMERICAL EXPERIMENT

The normalized quantitative outputs of the TE and TM polarizations from the right and upper ports in the MZI are plotted in Fig. 4(a). The excitation method is the same as in [15]. The applicable angular range of the input beam of the PBS is determined by the EFCs of the selected PhC. As shown in Fig. 2(a), ±6° divergence from the surface normal can be self-collimated for both polarizations. As is well known, the spatial divergence of a beam is related with its wavelength and width [17]. We thus set the width of the input beam to $8a$. This width represents ±6° divergence of the incident beam [18], within which TE- and TM-polarized waves can be self-collimated by the PBS. If the input beam is narrower than $8a$, its divergent angle would be larger than 12° and part of its spatial components would not be self-collimated. The efficiency of the device would then be degraded because the interference condition at the output port could not be satisfied.

It is observed that ~96% of the TE polarization travels out from the right port with only ~0.9% TM cross talk. The response is flat in the SC frequency region. On the other hand, the TM polarization directly travels out from the upper port with 4% TE cross talk. The different cross talk between TE and TM polarizations originates from the splitting mechanism. The TE polarization is suppressed at the upper port by the destructive interference and thus its cross talk at the upper port is very small. For the TM polarization, the reflections at the two air slits are mainly suppressed by the optical tunneling. Therefore, its cross talk at the right port is relatively larger. As the operating wavelength ($\sim 5a$) is much larger than the width of the two slits ($\sim 0.1a$) and the two arms of the MZI are symmetric, the difference of the optical path between the

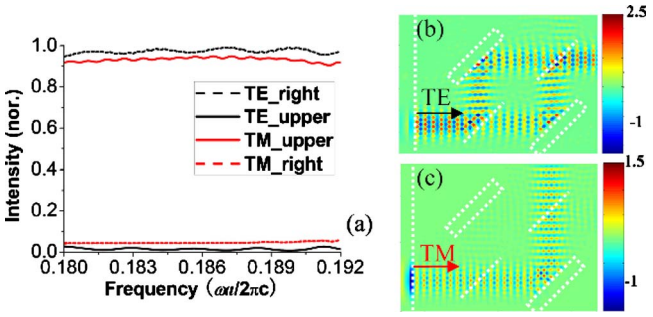

Fig. 4. (Color online) (a) The quantitative outputs of both polarizations for the upper and right ports, which are normalized to the power at the position of the green dashed line in Fig. 2(b). The solid (dashed) lines represent the output at the upper (right) port. (b) The H-field and (c) E-field distributions at a frequency of $0.188 \times 2\pi c/a$ for TE and TM polarizations. The input interface, reflecting mirrors, and air slits are outlined by the white dashed lines.

two arms is the same at different frequencies and thus the outputs are similar over the SC frequency range. Therefore, the two polarizations can be separated over a wavelength bandwidth as broad as ~100 nm at 1550 nm as shown in Fig. 4(a). This broad wavelength range can provide a very large fabrication tolerance for the device. Furthermore, as the width of the slit is much smaller than the operating wavelength, the outputs of the PBS are not sensitive to the variation of the slit's position relative to the center of pill-shaped holes (results will be presented in the next section).

The field distributions in the MZI at a normalized frequency of $0.188\times 2\pi c/a$ are given in Figs. 4(b) and 4(c). Obviously, the TE-polarized beam travels out from the right port and TM from the upper one, as we have analyzed in the above context.

4. DISCUSSIONS ON THE INFLUENCE OF INTERFACES

In the above context, we have demonstrated the polarization splitting function of the PBS and its efficiency without considering the effect of interfaces. Interfaces are very important factors to influence the performance of devices based on PhCs. First of all, the termination of the PhC can significantly affect the input/output coupling efficiency of the device [19]. It could be improved by applying suitable impedance matching layers at the interface. As it is difficult to minimize the reflections for both polarizations simultaneously by an impedance matching layer, we optimize it in such a way that the reflections are relatively low for both polarizations at a frequency. The method utilized is similar to that proposed in [20]. The parameters of the impedance matching layer are outlined as in Fig. 5(a), in which $r_1=0.44a$, $d_1=0.6a$, $r_2=0.5a$, and $d_2=0.5a$. The normalized quantitative outputs of the TE and TM polarizations from the right and upper ports in the MZI (including the effects of the input/output interface) are plotted in Fig. 5(b). As can be seen, about 96.7% (91%) of the TE (TM) polarization travels out from the right (upper) port at a normalized frequency of $0.186\times 2\pi c/a$. This relatively high transmission suggests that the interference condition has not been changed even with the sharp interface at this frequency. At other frequencies, the performance of the PBS would, however, be degraded by the unwanted reflections of the interfaces. The periodic oscillations of the transmissions are due to the periodic matching of the impedance matching layer. Therefore, the reflections of the input and output interfaces will reduce the efficiency of the PBS. To realize high transmissions for both polarizations in a wide frequency range, the impedance matching layer has to be designed very carefully. This issue is out of the range of our present paper and will be investigated in the future work.

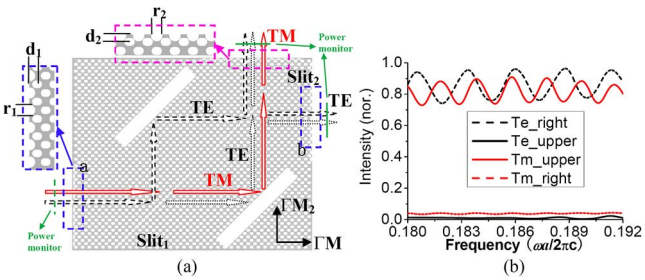

Fig. 5. (Color online) (a) Sketch map of the finite PBS. The dashed squares highlight the position of the impedance matching layers and their details are shown in the insets. Dashed squares a and b are the same. r_i stands for the radius of the outmost semicircles and d_i denotes the distance between the outmost semicircles and the second outmost pill-voids. The green lines represent the positions of the power monitor. (b) The quantitative outputs of both polarizations for a finite PBS, which are normalized to the input sources. The solid (dashed) lines represent the output at the upper (right) port, respectively.

Secondly, the slits' position relative to the pill-void center may influence the performance of the PBS. We scan the position of one of the slits with another one fixed in the range of $\pm 0.2a$. The results are plotted in Fig. 6. It is obvious that the outputs of the PBS remain similar even with $0.2a$ shift from the pill-shaped holes' center. This is because that the operation wavelength ($\sim 5a$) is much larger than the width of the slits ($\sim 0.15a$), as we have pointed out in Section 3.

The position of the reflection mirrors (RMs) will also affect the outputs of the MZI. In our modeling, we set the two RMs at the same position (relative to the nearest void) to provide symmetric MZI arms.

At last, the shape of the void will influence the performance of the PBS significantly. The advantage of the proposed PBS based on the pill-shaped void with square lattice geometry is that the TE/TM polarizations cannot only be separated but also be self-collimated. Furthermore, it operates in the first band. Therefore, both in-plane and out-of-plane diffraction losses can be suppressed simultaneously. PBS in PhC based on other lattice geometries or other shapes of voids does not have similar advantages.

5. CONCLUSIONS

To summarize, we have constructed a self-collimating polarization beam splitter (PBS) with the configuration of a Mach–Zehnder interferometer (MZI) consisting of the polarization-independent PhCs. The splitting mechanism is based on the phenomenon that TE/TM polarizations respond distinctly when encountering dielectric boundaries. TE and TM polarizations can be separated by 90° over the self-collimating frequency range (~6.5%) in a structure as short as 13 μm. The cross talk for TM (TE) polarization is

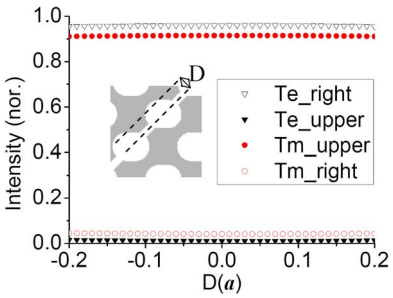

Fig. 6. (Color online) The dependence of the output of the MZI on the position shift of the slit relative to the holes' center. During the simulation, the position of one slit is scanned while another one fixed. The normalized frequency used in the simulation is $0.186\times 2\pi c/a$. The inset denotes the details of the displacement of the slit.

as low as 0.9% (4%). It has been found that the termination of the photonic crystal (PhC) could reduce the efficiency of the PBS due to the reflections. This PBS is suitable for photonic integrations because of its broad operating bandwidth and non-diffractive propagation.

ACKNOWLEDGMENTS

The authors acknowledge the financial support from the National Natural Science Foundation of China (NSFC) (Grants No. 10774050 and No. 10974060) and the Program for Innovative Research Team of the Higher Education in Guangdong (Grant No. 06CXTD005).

REFERENCES

1. S. M. Garner, V. Chuyanov, S. Lee, A. Chen, W. H. Steier, and L. R. Dalton, "Vertically integrated waveguide polarization splitters using polymers," IEEE Photon. Technol. Lett. **11**, 842–844 (1999).
2. L. Wu, M. Mazilu, J. F. Gallet, T. F. Krauss, A. Jugessur, and R. M. De La Rue, "Planar photonic crystal polarization splitter," Opt. Lett. **29**, 1620–1622 (2004).
3. X. Ao and S. He, "Polarization beam splitters based on a two-dimensional photonic crystal of negative refraction," Opt. Lett. **30**, 2152–2154 (2005).
4. X. Ao, L. Liu, L. Wosinski, and S. He, "Polarization beam splitter based on a two-dimensional photonic crystal of pillar type," Appl. Phys. Lett. **89**, 171115 (2006).
5. E. Schonbrun, Q. Wu, W. Park, T. Yamashita, and C. J. Summers, "Polarization beam splitter based on a photonic crystal heterostructure," Opt. Lett. **31**, 3104–3106 (2006).
6. H. Kosaka, T. Kawashima, A. Tomita, M. Notomi, T. Tamamura, T. Sato, and S. Kawakamib, "Self-collimating phenomena in photonic crystals," Appl. Phys. Lett. **74**, 1212–1214 (1999).
7. J. Witzens, M. Loncar, and A. Schere, "Self-collimation in planar photonic crystals," IEEE J. Sel. Top. Quantum Electron. **8**, 1246–1257 (2002).
8. L. Wu, M. Mazilu, and T. F. Krauss, "Beam steering in planar-photonic crystals: From superprism to supercollimator," J. Lightwave Technol. **21**, 561–566 (2003).
9. D. W. Prather, S. Shi, D. M. Pustai, C. Chen, S. Venkataraman, A. Sharkawy, G. J. Schneider, and J. Murakowski, "Dispersion-based optical routing in photonic crystals," Opt. Lett. **29**, 50–52 (2004).
10. V. Zabelin, L. A. Dunbar, N. Le. Thomas, R. Houdré, M. V. Kotlyar, L. O'Faolain, and T. F. Krauss, "Self-collimating photonic crystal polarization beam splitter," Opt. Lett. **32**, 530–532 (2007).
11. Y. Xu, X. Chen, S. Lan, Q. Dai, Q. Guo, and L. Wu, "Polarization-independent self-collimation based on pill-void photonic crystals with square symmetry," Opt. Express **17**, 4903–4912 (2009).
12. M. G. Moharam, D. A. Pommet, E. B. Grann, and T. K. Gaylord, "Stable implementation of the rigorous coupled-wave analysis for surface-relief gratings: Enhanced transmittance matrix approach," J. Opt. Soc. Am. A **12**, 1077–1086 (1995).
13. D. Zhao, J. Zhang, P. Yao, X. Jiang, and X. Chen, "Photonic crystal Mach–Zehnder interferometer based on self-collimation," Appl. Phys. Lett. **90**, 231114 (2007).
14. S. G. Johnson and J. D. Joannopoulos, "Block-iterative frequency-domain methods for Maxwell's equations in a planewave basis," Opt. Express **8**, 173–190 (2001).
15. X. Yu and S. Fan, "Bends and splitters for self-collimated beams in photonic crystals," Appl. Phys. Lett. **83**, 3251–3253 (2003).
16. S. D. Gedney, "An anisotropic perfectly matched layer-absorbing medium for the truncation of FDTD lattices," IEEE Trans. Antennas Propag. **44**, 1630–1639 (1996).
17. D. Deng, "Nonparaxial propagation of radially polarized light beams," J. Opt. Soc. Am. B **23**, 1228–1234 (2006).
18. H. A. Haus, *Wave and Fields in Optoelectronics* (Prentice-Hall, 1984).
19. Y. A. Vlasov and S. J. McNab, "Coupling into the slow light mode in slab-type photonic crystal waveguides," Opt. Lett. **31**, 50–52 (2006).
20. S.-G. Lee, J.-s. Choi, J.-E. Kim, H.-Y. Park, and C.-S. Kee, "Reflection minimization at two-dimensional photonic crystal interfaces," Opt. Express **16**, 4270–4277 (2008).